^{1}H MAS NMR Study of Local Structure and Dynamics of Water Molecule in (±)-[Co(en)$_3$]Cl$_3$·*n*D$_2$O

Takahiro Ueda* and Nobuo Nakamura†

The Museum of Osaka University, and Department of Chemistry, Graduate School of Science, Osaka University, Toyonaka, Osaka 560-0043, Japan

Received: December 29, 2002; In Final Form: July 2, 2003

Dependence of the local structure and dynamic behavior of hydration water in (±)-[Co(en)$_3$]Cl$_3$·*n*D$_2$O crystal ($0 \le n \le 4$) on the dehydration process was studied by means of ^{1}H magic-angle sample spinning (MAS) NMR technique. The line shape in the ^{1}H MAS NMR spectrum depends strongly on the water content (*n*). For $n < 1.5$, the spectrum consists mainly of two peaks whose relative intensities change with *n*, suggesting that the hydration water forms two different types of domainlike structures at room temperature. In addition, the full width at half-maximum of each component of the doublet was less than 1 ppm at room temperature, implying that the water moves rapidly enough to reduce the intermolecular ^{1}H−^{1}H dipole interaction. On cooling, the resonance line broadens and its line width exceeds 10 ppm below 200 K where the components of the doublets cannot be discerned. This aspect suggests that the water molecule undergoes slower motion than the MAS rate (5.0−7.0 kHz). The temperature dependence of the line width was analyzed by assuming the Davidson−Cole's spectral density. The activation energy (E_a) for the molecular motion of the water depends drastically on the water content: E_a assumes the constant value of 24 kJ mol^{-1} for $n \le 2.1$, but it decreases continuously for $n > 2.1$ and reaches 18 kJ mol^{-1} at $n = 4$. This finding suggests that the molecular motion of hydration water in the pore, which averages out the dipolar interaction between a trace amount of HDO and the protons on the pore wall, changes from whole molecular translational jump to proton migration through hydrogen bond accompanied by molecular reorientation.

1. Introduction

Several porous materials with micropores as well as mesopores have recently been synthesized and have increasingly been used as ion-exchange agents, molecular sieves, catalysts, catalyst supports, and reaction fields.[1−3] To improve the quality of the porous materials and to give a high selectivity to the catalytic reaction, it is necessary to understand thoroughly the interaction between the host porous materials and the guest molecules as well as the static and dynamic behavior of the guests in pores. An extremely uniform or periodically homogeneous pore makes it possible to investigate the interaction between the pore and the guest molecules in detail, because the positions of the guest molecules are uniquely identified in such a homogeneous pore. Such a system may provide clues for quantitative discussion of the structure and the dynamics of guest molecules in the process of the adsorption and desorption.

Typical and most popular porous materials are zeolites which are composed of sodium silicates or sodium aluminosilicates; the shape and the size of zeolitic pores depend strongly on the synthetic condition and the composition.[4] A great number of studies on the structure and the dynamics of guest molecules in the zeolitic pores have been carried out so far.[5−10] However, those compounds cannot provide uniform and homogeneous nanochannels because some distortion or structural disorder may inevitably be brought into the material in the synthetic processes. It has been also known that the crystals of some organic compounds possess ideal nanochannels.[11,12] In these cases, however, the pore structure changes often with the amount of the adsorbed guest molecules because of the softness of the framework of organic host crystal. Recently, new porous materials were synthesized on the basis of the metal complexes with some organic compounds and of the organic/inorganic hybride compounds.[13−16] However, it was reported that the pore structure in some of those compounds may be changed when the guest molecules are accommodated. Therefore, any ideal, homogeneous nanochannel for the quantitative study of the host−guest as well as guest−guest interactions has not hitherto been available.

Tris(ethylenediamine)cobalt(III) chloride, [Co(en)$_3$]Cl$_3$, is well known as a prototypal low-spin diamagnetic cobalt d^6 (t_{2g}-6) complex. This compound usually crystallizes from water as a racemic hydrated crystal, (±)-[Co(en)$_3$]Cl$_3$·*n*H$_2$O, $n \sim 3$. The crystal of a very usual metal complex compound, (±)-[Co(en)$_3$]Cl$_3$·*n*H$_2$O, has extremely uniform and homogeneous nanochannels in its structure. (±)-[Co(en)$_3$]Cl$_3$·*n*H$_2$O crystallizes in a trigonal $P\bar{3}c1$ unit cell with $a = (1.150 \pm 0.002)$ nm, $c = (1.552 \pm 0.004)$ nm, and $Z = 4$ at 290 K.[17,18] A straight nanochannel extends along the *c*-axis, and it can accommodate hydration water molecules up to 4 per formula unit (16 per unit cell). Three water molecules can occupy the 12g positions in an *ab*-plane, and each of 0.5 molecules can occupy 2a and 2b positions in the nanochannel as shown schematically in Figure 1. The water molecules are weakly linked together with hydrogen bonds. The sorption and desorption processes of the hydration water are characterized macroscopically by the capillary condensation and so the water is thought to have a

* Address correspondence to this author. Phone: +81-6-6850-5779; fax: +81-6-6850-5785; e-mail: ueda@museum.osaka-u.ac.jp.

† Present address: Department of Chemistry, Graduate School of Science and Technology, Shinshu University, Matsumoto, Nagano 390-8621, Japan.

10.1021/jp027847x CCC: $25.00
Published on Web 11/15/2003

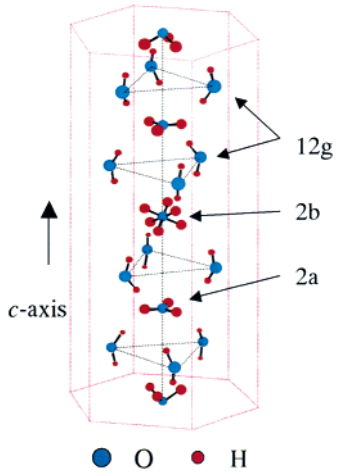

Figure 1. Schematic representation of the water arrangement in the nanochannel of (±)-$[Co(en)_3]Cl_3 \cdot nH_2O$. a and b denote the distinguishable special positions and g a general position. The number before a symbol means the number of the available sites in the unit cell.

"zeolitic" property.[19] Very recently, we found that the water accommodated in the pore of this substance can be substituted for some organic chain molecules such as *n*-alkanes, *n*-alcohols, *n*-alkylamines, and acetonitrile with no destruction of the crystal lattice.[20] We also carried out ^{129}Xe NMR measurements on this compound to examine the pore structure. The isotropic ^{129}Xe chemical shift at zero pressure led to a pore diameter of 0.44 nm.[21] Furthermore, ^{59}Co NMR and X-ray diffraction measurements using single-crystal recently confirmed that the dehydration process occurs without significant changes to the crystal lattice.[22] Thus, this compound is expected to be a new candidate for the material which provides an ideal, homogeneous nanochannel. However, the hydration and dehydration processes of this compound together with the experimental condition for the possible substitution of the water for organic molecules have not been studied from the microscopic point of view. To ensure such substitution for any small organic molecules, it is necessary to investigate closely the molecular behavior and the local structure of the hydration water in the dehydration processes.

The molecular motion of the water in this compound was studied by a dielectric measurement[23] and a solid-state NMR.[24] The dielectric measurement found that the water molecules undergo hindered rotation between −150 °C and room temperature. It was also predicted that the proton jump along the crystallographic *c*-axis through the hydrogen-bonded network takes place. Our previous work studied the static and dynamic properties of hydration water in (±)-$[Co(en)_3]Cl_3$ by means of ^1H, ^2H, and ^{17}O solid-state NMR. The ^1H pulsed field gradient (PFG) NMR revealed that some water molecules undergo diffusive motion through a nanochannel along the *c*-axis. The ^2H NMR spectrum at room temperature indicated the existence of a finite quadrupole interaction which is attributable to the rapid rotation of water molecule about its C_2-axis. The ^{17}O NMR spectrum consists of a narrow Gaussian peak and a broad powder pattern, suggesting that the water molecules are distributed among the general 12g positions and the special 2a and 2b positions. However, the activation parameters such as the activation energy and the correlation time for the motion of the hydration water have not yet been evaluated, though these parameters are important in the study of the molecular mechanism of absorption and desorption of the water molecules in the ideal regular nanochannels in the substance.

In the present work, we measure ^1H solid-state high-resolution NMR spectrum of HDO species accommodated in the nanochannel of (±)-$[Co(en)_3]Cl_3 \cdot nD_2O$ with different water contents between $n = 0.25$ and 4.0 to study the local structure of the water molecules in a nanochannel. For H_2O in the rigid lattice such as $CaSO_4 \cdot 2H_2O$, the line broadening of the ^1H stationary NMR spectrum is mainly caused by the intramolecular $^1H-^1H$ dipolar interaction, which brings about the line width of more than 45 kHz (∼10.8 G).[25] Although magic-angle sample spinning (MAS) technique enables principally to eliminate the large intramolecular $^1H-^1H$ dipolar interaction with using the fast spinning rate comparable to the line width (∼45 kHz), this is quite a hard condition to achieve experimentally. To solve this difficulty, our idea is to use a HDO molecule to acquire the ^1H high-resolution NMR spectrum. Even for HDO molecule in the rigid lattice, the intramolecular $^1H-^2H$ dipolar interaction (∼6.8 kHz) is much smaller than the intramolecular $^1H-^1H$ dipolar interaction because of the small gyromagnetic ratio of ^2H (ca. $\gamma(^2H)/\gamma(^1H) \sim 0.15$). In addition, the intermolecular $^1H-^1H$ dipolar interaction between the neighboring HDO molecules will be contributed to the line broadening. However, the large $^1H-^1H$ distance between the neighboring HDO molecules gives small contribution of the intermolecular $^1H-^1H$ dipolar interaction to the line width. For example, the intramolecular $^1H-^1H$ distance for water occupying 12g site is 0.139 nm, where the intermolecular O−O distance between nearest neighboring 12g waters is 0.381 nm.[18] Assuming that the intermolecular $^1H-^1H$ distance is approximately equal to the intermolecular O−O distance between nearest neighboring 12g waters, the intermolecular $^1H-^1H$ dipolar interaction is estimated to be only 5% (∼2.3 kHz) of the intermolecular $^1H-^1H$ dipolar interaction. Thus, it is expected that the conventional MAS probe, which can achieve the sample spinning rate up to 10 kHz, can be used to eliminate the intramolecular $^1H-^2H$ dipolar interaction (∼6.8 kHz) as well as the intermolecular $^1H-^1H$ dipolar interaction (∼2.3 kHz). The ^1H high-resolution spectrum for HDO in (±)-$[Co(en)_3]Cl_3 \cdot nD_2O$ will provide us the information about the chemical environments of HDO such as the hydrogen bond.

We also examine the temperature dependence of the line width of the ^1H resonance under the MAS condition. The line width of the ^1H resonance of HDO in (±)-$[Co(en)_3]Cl_3 \cdot nD_2O$ is expected to be a good probe to detect the proton jump as well as the translational motion and migration of a whole water molecule, since the intermolecular $^1H-^1H$ dipolar interaction is modulated by only molecular motion which varies the intermolecular $^1H-^1H$ distances. In contrast, ^2H NMR is very sensitive for the fluctuation of the electric field gradient (EFG) around ^2H nuclei. Since it is assumed that the principal axis of the EFG tensor approximately lies along the D−O bond in D_2O, the EFG tensor is effectively modulated by rotation or reorientation of the heavy water molecule. On the other hand, orientation of the EFG tensor to the external magnetic field is invariant when ^2H nuclei are moved only by translation. That is, the translational motion and migration little affect the ^2H NMR spectrum broadened by the quadrupole interaction. Thus, probing the intermolecular $^1H-^1H$ dipolar interaction in (±)-$[Co(en)_3]Cl_3 \cdot nD_2O$ through the line width of ^1H MAS NMR spectrum provides us the information of molecular dynamics such as the proton jump, the translational motion, and the migration of HDO in the nanochannel.

2. Experimental Section

2.1 Sample Preparation. (±)-$[Co(en)_3]Cl_3$ was synthesized according to literature.[17] The crystalline sample was obtained by repeating the recrystallization three times from aqueous solution. The anhydrates were prepared by drying

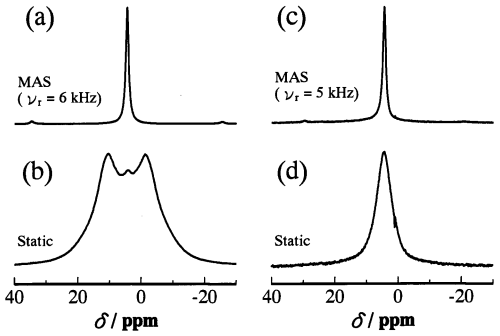

Figure 2. ^{1}H NMR spectra for (±)-[Co(en)$_3$]Cl$_3$·3.0H$_2$O observed under MAS (a) and static (b) conditions, and for (±)-[Co(en)$_3$]Cl$_3$·3.0D$_2$O observed under MAS (c) and static (d) conditions. ν_r denotes the MAS rate. All the spectra were measured at room temperature.

(±)-[Co(en)$_3$]Cl$_3$·nH$_2$O at 120 °C under ambient pressure for 3 days. (±)-[Co(en)$_3$]Cl$_3$·4D$_2$O was prepared by storing the anhydrate under the atmosphere of D$_2$O (≥99.8%, Wako Pure Chemical Industries, Ltd.) for 3 days. Each of the samples with different water contents was prepared by keeping (±)-[Co(en)$_3$]-Cl$_3$·4D$_2$O at 120 °C for some time under ordinary atmosphere to establish partial dehydration; the amount of water in the sample was then determined to within ±10% by measuring weight of the sample.

2.2 NMR Measurement. NMR measurements were carried out using Bruker Model DSX-200 pulsed NMR spectrometer operating at the Larmor frequency of 200.13 MHz for proton. MAS NMR spectra were acquired with Bruker 4 mmϕ high-speed MAS probe at the sample spinning rate between 5.0 and 7.0 kHz. The temperature of sample was controlled using Bruker BVT-3000 unit to within ±1 K by heating or cooling the bearing gas. The temperature of sample was calibrated against the temperature dependence of ^{207}Pb resonance frequency in Pb(NO$_3$)$_2$.[26−28] The chemical shift of ^{1}H was referred to the ^{1}H resonance of TMS.

3. Result and Discussion

3.1 ^{1}H MAS NMR Spectrum in (±)-[Co(en)$_3$]Cl$_3$·nD$_2$O. Figure 2 shows the ^{1}H NMR spectra of (±)-[Co(en)$_3$]Cl$_3$·3.0H$_2$O and (±)-[Co(en)$_3$]Cl$_3$·3.0D$_2$O observed at room temperature under the magic-angle spinning (MAS) and static conditions. The powder spectrum for (±)-[Co(en)$_3$]Cl$_3$·3.0H$_2$O under static condition spreads over 20 ppm (∼4 kHz) and has a characteristic structure of a weak dipolar interaction in the isolated ^{1}H−^{1}H pair. The ^{1}H NMR spectrum of (±)-[Co(en)$_3$]Cl$_3$·3.0D$_2$O has no structure since in this substance most of the water protons exist as HDO (the protons of 99% are in the form of HDO in D$_2$O (99%)), and so the ^{1}H−^{1}H dipolar interaction is negligible. This finding implies that the ^{1}H NMR spectrum detects mainly the resonance due to the water accommodated in the pore. The ^{1}H signal from ethylenediamine coordinated to cobalt(III) ion, in which the rigid CH$_2$ group is expected to be Pake doublet with the peak separation of ∼38 kHz, may be broadened out by the strong ^{1}H−^{1}H dipolar interaction. Furthermore, the fact that the intramolecular ^{1}H−^{1}H dipolar interaction in a water molecule can be observed in the nondeuterated specimen at room temperature indicates that the molecular motion of water works to average out the intramolecular dipolar interaction only partially. The rotation or reorientation of water around the C_2 axis as observed in the ^{2}H NMR spectra[24] just reduces the intramolecular ^{1}H−^{1}H dipolar interaction by a factor of 2. The narrow doublet with separation of ∼4 kHz for (±)-[Co(en)$_3$]Cl$_3$·3.0H$_2$O observed under the stationary condition implies that the molecular motion such as the proton jump, the translational motion, and the migration of a whole water molecule takes place in addition to the rotational motion about the C_2 axis of water. This molecular motion is also fast enough to average out the ^{1}H chemical shift anisotropy about 30−40 ppm (6−8 kHz at 4.7 T magnetic field) in ice,[29] because this reduces the intermolecular ^{1}H−^{1}H dipolar interaction of ∼45 kHz to be only ∼4 kHz.

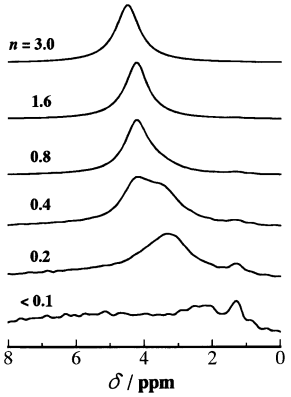

Figure 3. ^{1}H MAS NMR spectrum of (±)-[Co(en)$_3$]Cl$_3$·nD$_2$O measured with the MAS rate of 5 kHz at 293 K. The water content (n) was changed between 3.0 and 0.1.

The narrow and weak line observed between the doublet of ^{1}H stationary spectrum will come from the trace amount of the surface water as observed on the ^{2}H NMR spectrum in the previous study.[24] In our previous ^{2}H NMR study for (±)-[Co(en)$_3$]Cl$_3$·nD$_2$O, the spectra observed below 162 K for $n \geq 3$ consist of two resonance lines with quite different quadrupole coupling constant (QCC). The difference in the site symmetry between 12g general position (QCC = 226 ± 2 kHz) and 2a and 2b special positions (QCC ∼ 0 kHz) enables to distinguish two resonance lines. At room temperature, the exchange of heavy water between these sites brings about small quadrupole coupling constant (∼4.5 kHz). In this study, however, the proton jump between the neighboring water molecules as well as the translational motion and the migration of a whole water molecule, in addition to the rapid rotation or reorientation, average both the line shapes and the isotropic chemical shift values for ^{1}H in HDO occupying the different crystallographic sites. As a result, the ^{1}H stationary spectrum at room temperature is observed as the weighted average between the resonance lines from water located at 12g and 2a (2b) sites.

Thus, the MAS technique enables to eliminate the residual dipolar interaction completely, giving a narrow spectrum with the line width of less than 1 ppm. This technique makes it possible to study the dynamical structure of water molecules accommodated in nanochannels.

3.2 Dependence of ^{1}H Chemical Shift on Water Content. Figure 3 shows the dependence of the ^{1}H MAS NMR spectrum of (±)-[Co(en)$_3$]Cl$_3$·nD$_2$O at 293 K on the water content n in the range between n = 3.0 and 0.1. A structureless peak is observed at 4.3 ppm for $n > 1.6$, but a small shoulder and a small peak appear at about 3.5 and 1.3 ppm, respectively, for $n < 1.6$. They grow up gradually with decrease in the water content, whereas the peak at 4.3 ppm disappears for $n < 0.2$. The peak at 1.3 ppm becomes dominant for $n < 0.1$.

The value of the ^{1}H chemical shift in bulk water has conveniently been interpreted in terms of the hydrogen bonding among water molecules.[30] The hydrogen bond elongates the O−H distance, resulting in the decrease in the electron density

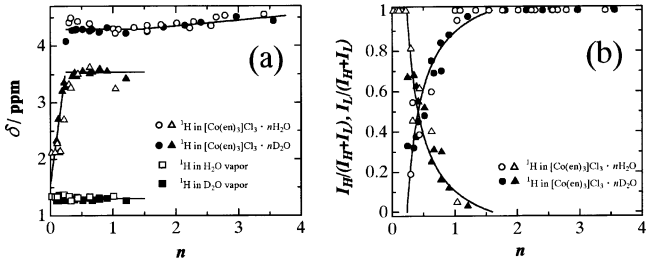

Figure 4. The water content dependence of (a) ^{1}H chemical shift values for three main components and (b) the relative intensities of the peaks at 4.3 and 3.6 ppm in the ^{1}H MAS NMR spectra of (±)-[Co(en)$_3$]Cl$_3$·nH$_2$O and (±)-[Co(en)$_3$]Cl$_3$·nD$_2$O.

on the proton. Then, the protons which are engaged in the hydrogen bond formation are more de-shielded than those in the free molecules.[31] Because of the rapid exchange of protons in the bulk water, we can observe only the averaged value between the ^{1}H chemical shifts for the hydrogen-bonded waters and the free ones. The ^{1}H chemical shift values have been known to distribute over 3.9−5.2 ppm in bulk water, depending on the relative number of the hydrogen-bonded species.[32] For water molecules in the vapor or in CCl_4 and cyclohexane in which the water rarely contributes to the hydrogen bond, the δ value is less than 1 ppm.[32] This value may be attributed to the proton chemical shift for completely free water molecule.

By referring to the above experimental results on the hydrogen bonding in water, we tried to derive from our NMR data in Figure 3 quantitative information on the static and dynamic behavior of hydrogen-bonded water molecules accommodated in the homogeneous one-dimensional nanochannel. First of all, we deconvoluted the observed spectra in Figure 3 to several components with the Lorentzian line shape and evaluated the ^{1}H chemical shift values for the individual components as shown in Figure 4a.

When $n > 1.3$, the spectrum consists of a single peak which shifts linearly from 4.5 to 4.3 ppm as n decreases. This implies that the exchange of the protons between the hydrogen-bonded molecules and the free ones is fast enough to average their chemical shifts. The decrease in the averaged chemical shift value with decrease in n in this region implies that the number of hydrogen bonds tend to decrease with decrease in n.

In the region of the water content, $0.25 \leq n \leq 1.3$, the spectrum consists of three components at $\delta = 4.3$, 3.6, and 1.3 ppm. These chemical shift values are almost independent of n. The resonances at 4.3 and 3.6 ppm are attributed to the protons in hydrogen-bonded water of crystallization, whereas the peak at 1.3 ppm may be assigned to the vaporized water in equilibrium with the crystalline compound or to some water molecule which is almost free from hydrogen bonding. Since a hydrogen involved in a stronger hydrogen bond gives a larger chemical shift, the protons with the chemical shift of 4.3 ppm come from water molecules which are linked to each other to form strong hydrogen-bonded networks in the nanochannel, whereas those with $\delta = 3.6$ ppm come from water molecules which are weaker hydrogen-bonding. The fact that the two peaks are well-separated implies that the rate of the exchange between these protons is lower than 140 Hz (~0.7 ppm), suggesting that these water molecules come from the different components with the different water contents. The probability for the exchange of protons between these different components will depend on the amount of the components, the size of crystallites, and the mobility of the proton in each component. Especially, the size of the crystallites would be much larger than the mean-free path of the protons, and the exchange rate of the water molecules between the crystallites of the different components will be lower.

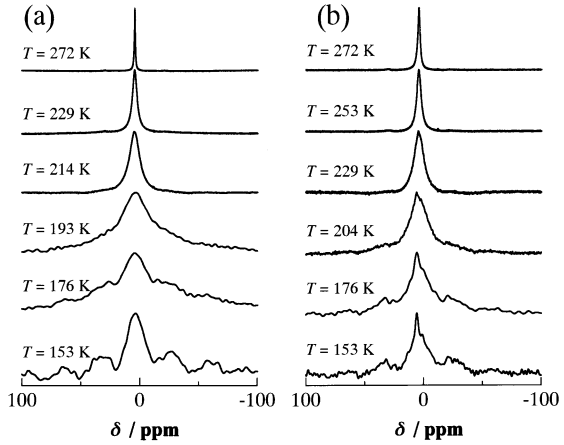

Figure 5. Temperature dependence of ^{1}H MAS NMR spectra of (±)-[Co(en)$_3$]Cl$_3$·nD$_2$O with $n = 2.3$ (a) and 3.7 (b). The MAS rate is 5 kHz.

The above idea may interpret the dependence of the relative integrated peak intensities on the water content. When n decreases, the normalized intensity of the peak at $\delta = 4.3$ ppm (I_H) by the total intensity ($I_H + I_L$) decreases whereas that at $\delta = 3.6$ ppm (I_L) increases as shown in Figure 4b. When $n > 1.6$ all water molecules give the large chemical shift ($\delta = 4.3$ ppm), suggesting that they are tightly linked by strong hydrogen bonds, whereas when $n < 0.25$ all water molecules give the small chemical shift, implying that the water molecules are loosely linked to each other. In the range of $0.25 < n < 1.6$, the sample may be considered to be a mixture of two different components with the different water contents.

When $n < 0.25$, the peak at 4.3 ppm disappears and the peak at 3.6 ppm shifts to higher field with further decrease in n and is finally at 2.1 ppm when $n < 0.1$. This suggests that the decrease in n to 0.1 is accompanied by the dehydration of water of crystallization and by a decrease of the density of the water molecules in the pore and hence a decrease in the chance for the molecules to form hydrogen bonds. On the other hand, the chemical shift of the peak observed at the highest field, 1.3 ppm, remains constant irrespective of the value of n, implying that this resonance peak comes from the water vapor at the outside of the nanochannel, which is in equilibrium with water of crystallization.

3.3 Temperature Dependence of ^{1}H MAS NMR Spectra. Temperature dependence of ^{1}H MAS NMR spectra of (±)-[Co(en)$_3$]Cl$_3$·nD$_2$O with $n = 2.3$ and 3.7 is shown in Figure 5 (a) and (b), respectively. In both substances, the line width broadened from 1 to 20 ppm on cooling to 200 K, and below 200 K the spinning sidebands appeared at both sides of the central peak. The line width may be brought about by the residual dipolar interaction between the protons in water of crystallization and those in the surrounding host $[Co(en)_3]^{3+}$. In the presence of molecular motion, the dipolar interaction under the MAS condition is modulated by the molecular motion.[33] Then, the line width ($\Delta\nu_{MAS}$) is represented by

$$\Delta\nu_{MAS} = \left(\frac{C}{3\pi}\right)\left[J(\omega_r) + \frac{1}{2}J(2\omega_r)\right] \quad (1)$$

where C is the magnitude of the dipolar interaction which causes the line broadening, and $J(\omega)$ is the spectral density of the molecular motion. In general, $J(\omega)$ is the Fourier transform of

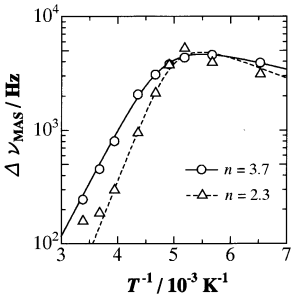

Figure 6. The temperature dependence of the line widths ($\Delta\nu_{MAS}$) in ^{1}H MAS NMR spectra of (±)-[Co(en)$_3$]Cl$_3$·nD$_2$O with n = 3.7 (○) and 2.3 (△). The solid and broken lines represent the theoretical line widths.

the Gaussian distribution of the correlation time, which gives a well-known BPP type spectral density function:[34]

$$J(\omega_r) = \frac{2\tau_c}{1 + \omega_r^2\tau_c^2} \tag{2}$$

where ω_r is the frequency of the sample spinning in radian/s unit, and τ_c the correlation time for the molecular motion.

According to this spectral density, when the rate of the molecular motion ($1/\tau_c$) becomes slower than the MAS rate ($1/\tau_c \ll \omega_r$), the line width is inversely proportional to the square of the MAS rate. When the rate of the molecular motion is comparable to the MAS rate, the efficiency of MAS is remarkably reduced, causing the maximum line broadening in the spectrum. For $1/\tau_c \gg \omega_r$, the line width is dominated only by the rate of the molecular motion and becomes narrower when the molecular motion becomes more rapid. Therefore, the temperature dependence of the line width in the ^{1}H MAS NMR spectrum provides us the information on the ultra slow motion (5.0−7.0 kHz in this work). We then carried out the line shape analysis at each temperature by assuming the Lorentzian function above 200 K and the Gaussian function below 200 K.[33] Figure 6 shows the temperature dependence of $\Delta\nu_{MAS}$ for the samples with n = 2.3 and 3.7. It is remarked that the maximum broadening occurs around 180−190 K and the slope at the higher temperature side of the maximum is much steeper than that at the lower temperature side. This fact implies that the correlation time for the molecular motion is widely distributed.[35]

To analyze the temperature dependence of the line width by taking account of the distribution in the correlation time, we apply the Davidson−Cole type spectral density to the motion of water molecules in the nanochannel of the present compound as follows:[36]

$$J(\omega_r) = \frac{2}{\omega_r}\left\{\frac{\sin[\epsilon \arctan(\omega_r\tau_c)]}{(1 + \omega_r^2\tau_c^2)^{\epsilon/2}}\right\} \tag{3}$$

where ϵ characterizes the distribution of the correlation time. When ϵ = 1 eq 3 is reduced to the BPP type spectral density, and the smaller the value of ϵ, the wider the distribution of the correlation time. The distribution width of τ_c is reflected in the sharpness of the slope in the $\Delta\nu_{MAS}$ versus $1/T$ plot below the temperature of the maximum broadening.

Assuming the Arrhenius activation process for the motion of the water in the pore, the temperature dependence of τ_c is represented by

$$\tau_c = \tau_0 \exp(E_a/RT) \tag{4}$$

TABLE 1: Activation Parameters for the Motion of Water in (±)-[Co(en)$_3$]Cl$_3$·nD$_2$O[a]

n	E_a/kJ mol^{-1}	C/10^9 rad^2 s^{-2}	τ_0/10^{-11} s	ϵ
0.45	24	5.0	4.5	0.05
0.63	24	5.0	4.0	0.05
1.1	24	4.0	2.8	0.08
1.8	25	3.5	1.5	0.1
2.3	24	3.0	1.8	0.15
3.0	20	2.0	32	0.16
3.7	18	3.2	100	0.13

[a] Determined by temperature dependence of line width of ^{1}H MAS NMR spectrum.

where E_a is the activation energy for the molecular motion and τ_0 is the preexponential factor. We analyzed the experimental line widths in Figure 6 using eqs 1, 3, and 4 and evaluated the activation parameters for two compounds with different n; the results obtained by the least squares method are listed in Table 1, and the calculated line widths are shown in Figure 6 for n = 2.3 and 3.7. The parameter C, which represents the strength of the dipolar interaction causing the line broadening, will bring about the motional mode of the water molecules. In the present specimens, protons exist as HDO molecules and hence the dipolar field which the proton in the guest HDO molecule experiences originates from the protons in the ethylenediamine in the host lattice. On the basis of the crystal structure of (±)-[Co(en)$_3$]Cl$_3$·2.7H$_2$O,[18] we estimated the strengths of the ^{1}H−^{1}H dipolar interactions between the guest water occupying the 12g general position and the 2a and 2b special positions and the host to be 3.8 × 10^9 rad^2 s^{-2} and 2.3 × 10^9 rad^2 s^{-2}, respectively. These values agree with the experimental C values recorded in Table 1, suggesting that the protons of water molecules in a pore undergo some motion that can average out the ^{1}H−^{1}H dipolar interactions between the host and the guest completely. To satisfy this condition, the protons in the water must undergo rapid translational motion in the straight pore; probable motion to establish it is the one-dimensional self-diffusion of the whole HDO molecule or proton transfer among the water molecules, which are arranged in the pore.

The preexponential factor in the Arrhenius equation, eq 4, corresponds to the correlation time at infinite temperature and so depends on the molecular motional mode. The τ_0 for the compound with $n \geq 3.0$ is larger by one or two orders than that with $n < 3.0$, suggesting that the motional mode of water in the pore is changed at the water content near n = 3.0. The motion becomes slower when the water content exceeds 3.0. This point is also supported by the analysis of the dependence of the activation energy on the water contents as described below.

The parameter ϵ characterizing the distribution of the correlation time τ_c is very small ($\epsilon < 0.2$) over whole water contents, indicating that τ_c is always distributed over an extremely wide range. This may come from two factors: one is the distribution of the local structure around water molecules because of some distortion of the basic structure, and the other is the generation of individual collective motions of various water clusters. At low water contents, the formation of defects at some water sites will bring about a great number of the configurations for the water arrangement, resulting in the variety of local structures around water molecules. On the other hands, at high water content, the water molecules will be packed together tightly and undergo a kind of collective motion that is generated by complicate coupling between rotation and translation, giving rise to a wide distribution of τ_c.

Finally, the activation energy (E_a) depends on the water content as can be seen in Table 1. In the range of n from 0 to

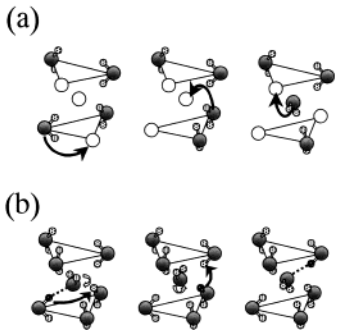

Figure 7. Schematic representation of motion of water molecule in the nanochannel of (±)-$[Co(en)_3]Cl_3$. At the water content below 2.1 (a), there are many defects on the water sites in the nanochannel, and the water molecules undergo the molecular jump between the unoccupied sites. On the other hand, at the water content above 2.1, the proton hopping takes place among the water molecules occupied, because the high occupation of the water molecules in the nanochannel decreases the probability of the molecular jump to the vacant sites.

2.1, the value of E_a is approximately a constant (24 kJ mol^{-1}). When $n > 2.1$, E_a decreases suddenly to 18 kJ mol^{-1}, suggesting that the mode of the water motion contributing to the ^{1}H line width is changed around $n = 2.1$. At $n \sim 0$, almost all available sites for water are vacant and the water molecules can easily jump among the vacancies. It is, however, almost impossible for the hydrogen atom or proton to move between different water molecules since hydrogen bonds which carry the proton jump are rarely formed. The increase in n leads to higher occupation of the vacant sites and hence causes increase in the hydrogen bonds between the water molecules in the pore. This situation may interpret the dependence of the ^{1}H chemical shift on the water content described above. At high water content, the hydrogen-bond network is established extensively, and so the protons can jump from one water molecule to another through the hydrogen bond in addition to the jump of water molecules as a whole. For the proton jump between the neighboring water molecules, there are two possible processes: one is the cooperative proton transfer through the hydrogen-bonding network, and the other is the formation of H_3O^+ and OH^- defects and reformation of H_2O. The proton jump taking place through both processes will work to average out the ^{1}H−^{1}H dipolar interaction at the high water content region. Since the proton jump accompanies lower activation energy than that for the jump of the water molecule as a whole, apparent activation energy is decreased with the increase in the frequency of the proton jump that is brought about by the increase in n.

The molecular motion of water confined in the mesoporous materials MCM-41 has recently been studied by quasi-elastic neutron scattering (QNS),[37] in which the activation energies for the translational and the rotational motions of water molecules were determined separately by selecting the appropriate range of the momentum transfer. It was reported that the E_a for the translation of water is 24−29 kJ mol^{-1} and for the rotation is 3.7−18 kJ mol^{-1}. Referring to these results, we can conclude that the water in the nanochannel in (±)-$[Co(en)_3]Cl_3$, $E_a = 24$ kJ mol^{-1} for $n < 2$ corresponds to some intersite jump of the water molecule and $E_a = 18$ kJ mol^{-1} observed at $n = 3.7$ to the proton (or hydrogen atom) jump through the hydrogen bond, the latter being associated with the reorientation of water molecules. The schematic representation of the molecular motion of water in the nanochannel is shown in Figure 7.

4. Conclusion

To investigate the dependence of the local structure and dynamics of heavy water in (±)-$[Co(en)_3]Cl_3 \cdot nD_2O$ on the dehydration process, we examined the line shape of ^{1}H MAS NMR spectrum as a function of the water content and temperature. By probing the trace of ^{1}H nucleus contained in heavy water, we can observe the well-resolved ^{1}H NMR signal for the hydration water. The dependence of ^{1}H chemical shift on water content suggests that the water molecules are classified to three different groups with respect to the manner of hydrogen bonding and that the exchange rate of protons between these groups is lower than the frequency difference between their signals (<140 Hz). In addition, the population of each group changes with water content.

Temperature dependence of ^{1}H MAS NMR spectrum suggests that water molecules undergo ultraslow motion below room temperature. The line width broadens on cooling to 20 ppm (∼4 kHz) at 200 K and becomes narrower again by further cooling. The analysis of the temperature dependence of the line width using the Davidson−Cole type spectral density leads to the activation parameters for the molecular motion of water in the pore. The activation energy shows the remarkable change with the water content: E_a is independent of water content (24 kJ mol^{-1}) for $0 < n \leq 2.1$ but decreases suddenly to 18 kJ mol^{-1} for $n > 2.1$. This finding suggests that the motional mode of water in the pore changes with the water content. Comparing the activation energy to that for the molecular motion of water confined in MCM-41, we can conclude that the molecular jump to the vacant sites in the pore takes place for $0 < n \leq 2.1$, whereas only the molecular reorientation at its fixed site is excited for $n > 2.1$. Thus, the migration of hydrogen atom in the pore takes place via molecular jump mechanism mediated by vacancies at water content lower than 2.1 and via hydrogen jump mechanism correlated to the molecular reorientation at water content higher than 2.1.

References and Notes

(1) Beck, J. S.; Vartuli, J. C.; Roth, W. J.; Leonowicz, M. E.; Kresge, C. T.; Schmitt, K. D.; Chu, C. T−W.; Olson, D. H.; Sheppard, E. M.; McCullen, S. B.; Higgins, J. B.; Schlenker, J. L. *J. Am. Chem. Soc.* **1992**, *114*, 10834.

(2) Epperlein, J. L.; Moore, J. G.; Landry, C. C. *Prepr. Pap.—Am. Chem. Soc., Div. Fuel Chem.* **1998**, *43*, 315.

(3) Inagaki, S.; Koiwai, A.; Suzuki, N.; Fukushima, Y.; Kuroda, K. *Bull. Chem. Soc. Jpn*. **1996**, *69*, 1449.

(4) Breck, D. W. *Zeolite Molecular Sieves*; John Wiley & Sons: New York, 1974 and references therein.

(5) Karger, J.; Ruthven, D. M. *Diffusion in Zeolites and other microporous solids*; John Wiley & Sons: New York, 1992.

(6) Xu, Q.; Eguchi, T.; Nakayama, H.; Nakamura, N. *J. Chem. Soc., Faraday Trans*. **1995**, *91*, 2949.

(7) Xu, Q.; Eguchi, T.; Nakayama, H.; Nakamura, N. *J. Chem. Soc., Faraday Trans.* **1996**, *92*, 1039.

(8) Xu, Q.; Eguchi, T.; Nakayama, H.; Nakamura, N. *J. Chem. Soc., Faraday Trans.* **1996**, *92*, 4601.

(9) Asanuma, T.; Nakayama, H.; Eguchi, T.; Nakamura, N. *J. Chem. Soc., Faraday Trans.* **1998**, *94*, 3521.

(10) Nagano, J.; Eguchi, T.; Asanuma, T.; Masui, H.; Nakayama, H.; Nakamura N.; Derouane, E. G. *Microporous Mesoporous Mater*. **1999**, *33*, 249.

(11) Allcock, H. R.; Levin, M. L.; Whittle, R. R. *Inorg. Chem.* **1986**, *25*, 41.

(12) Comotti, A.; Simonutti, R.; Stramare, S.; Sozzani, P. *Nanotechnology* **1999,** *10*, 70.

(13) Manakov, A. Yu.; Soldatov, D. V.; Ripmeester, J. A.; Lipkowski, J. *J. Phys. Chem*. **2000**, *B104*, 12111.

(14) Soldatov, D. V.; Ripmeester, J. A. *Chem. Mater*. **2000**, *12*, 1827.

(15) Kitagawa, S.; Kondo, M. *Bull. Chem. Soc. Jpn.* **1998**, *71*, 1739.

(16) Seki, K.; Takamizawa, S.; Mori, W. *Chem. Lett.* **2001**, 122.

(17) Nakatsu, K.; Saito, Y.; Kuroya, H. *Bull. Chem. Soc. Jpn.* **1956**, *29*, 428.

(18) Whuler, P. A.; Brouty, C.; Herpin, P. S. P. *Acta Crystallogr*. **1975**, *B31*, 2069.

(19) Chihara, H.; Nakatsu, K. *Bull. Chem. Soc. Jpn.* **1959**, *32*, 903.

(20) Nagaoka, N.; Ueda, T.; Nakamura, N. *Z. Naturforsch.* **2002**, *57a*, 435.

(21) Ueda, T.; Eguchi, T.; Nakamura, N.; Wasylishen, R. E. *J. Phys. Chem.* **2003**, *B107*, 180.
(22) Ueda, T.; Bernard, G. M.; McDonald, R.; Wasylishen, R. E. *Solid State Nucl. Magn. Reson.* **2003**, *24*, 163.
(23) Chihara, H.; Okawa, S.; Seki, *S. Bull. Chem. Soc. Jpn.* **1964**, *37*, 1373.
(24) Ueda, T.; Nakamura, N. *Z. Naturforsch.* **2000**, *55a*, 362.
(25) Abragam, A. *Principles of Nuclear Magnetism* Clarendon Press: New York, 1961; p 219.
(26) Bielecki, A.; Burum, D. P. *J. Magn. Reson.* **1995**, *A116*, 215.
(27) Isbester, P. K.; Zalusky, A.; Lewis, D. H.; Douskey, M. C.; Promije, M. J.; Mann, K. R.; Munson, E. J. *Catal. Today* **1999**, *49*, 363.
(28) Takahashi, T.; Kawashima, H.; Sugisawa, H.; Baba, T. *Solid State Nucl. Magn. Reson.* **1999**, *15*, 119.
(29) Werbelow, L. *J. Phys. Chem.* **1990**, *94*, 6663.
(30) Gutowsky, H. S.; Saika, A. *J. Chem. Phys.* **1953**, *21*, 1688.
(31) Sternberg, U.; Brunner, E. *J. Magn. Reson.* **1994**, *A108*, 142.
(32) Hindman, J. C. *J. Chem. Phys.* **1966**, *44*, 4582.
(33) Fenzke, D.; Gerstein, B. C.; Pfeifer, H. *J. Magn. Reson.* **1992**, *98*, 469.
(34) Bloembergen, N.; Purcell E. M.; Pound, R. V. *Phys. Rev.* **1948**, *73*, 679.
(35) Beckmann, P. A. *Phys. Rep.* **1988**, *171*, 86.
(36) Davidson, D. W.; Cole, R. H. *J. Chem. Phys.* **1951**, *19*, 1484.
(37) Takahara, S.; Nakano, M.; Kittaka, S.; Kuroda, Y.; Mori, T.; Hamano, H.; Yamaguchi, T. *J. Phys. Chem.* **1999**, *B103*, 5814.